

## Imaging Delocalized Electron Clouds: Photoionization of $C_{60}$ in Fourier Reciprocal Space

Andy Rüdél,<sup>1</sup> Rainer Hentges,<sup>1</sup> Uwe Becker,<sup>1,\*</sup> Himadri S. Chakraborty,<sup>2,†</sup> Mohamed E. Madjet,<sup>2</sup> and Jan M. Rost<sup>2</sup>

<sup>1</sup>*Fritz-Haber-Institut der Max-Planck-Gesellschaft, Faradayweg 4-6, D-14195 Berlin, Germany*

<sup>2</sup>*Max-Planck-Institut für Physik komplexer Systeme, Nöthnitzer Strasse 38, D-01187 Dresden, Germany*

(Received 3 April 2002; published 30 August 2002)

The dynamics of the photoionization of the two outermost orbitals of  $C_{60}$  has been studied in the oscillatory regime from threshold to the carbon  $K$  edge. We show that geometrical properties of the fullerene electronic hull, such as its diameter and thickness, are contained in the partial photoionization cross sections by examining ratios of partial cross sections as a function of the photon wave number in the Fourier conjugated space. Evaluated in this unconventional manner photoemission data reveal directly the desired spatial information.

DOI: 10.1103/PhysRevLett.89.125503

PACS numbers: 61.48.+c, 33.80.Eh, 36.40.Cg

Fullerenes, in particular  $C_{60}$  [1], are a very specific form of matter which causes surprising behavior even in such matured fields as scanning tunneling microscopy [2] and photoelectron emission [3], both well established tools for the structural analysis of matter. Because of its spherical symmetry a sample of  $C_{60}$  molecules provides all structural information independently from any particular orientation, either in crystalline form or in the gas phase [4]. This made it promising to look for such information in the dynamics of the photoionization cross sections of  $C_{60}$  and other fullerenes, particularly because theoretical considerations based on the acceleration form of the dipole operator showed that spatial regions with a large gradient in the potential of an illuminated target contribute dominantly to photoionization. The path differences of electron continuum waves emanating from these regions of steep potential gradient should lead to characteristic oscillatory patterns in the cross sections from which spatial properties of the target should be reconstructed.

Evidence for an oscillating behavior of the partial cross sections in fullerenes was first obtained from photoemission experiments on solid  $C_{60}$  by Benning *et al.* [5]. These early measurements showed a photon energy dependent oscillation in the intensity of the photolines of the two highest occupied molecular orbitals [(HOMO) and HOMO - 1] in the photon energy range between 24 and 100 eV whose origin was unknown. It has been attributed to a particular band structure in the continuum influenced by the special symmetries of the  $C_{60}$  bound states [5]. Only after the first gas phase measurements revealed similar oscillations [6] it became clear that this effect was not related to the electronic properties of condensed matter. However, also quantum chemical approaches based on individual electronic orbitals treating  $C_{60}$  as a big molecule failed to explain the origin of the oscillations. Xu, Tan, and Becker [7] explained the oscillations with an empirical refraction model where a valence electron inside the fullerene, modeled as a sphere of radius  $R$ , feels a constant potential. At the fullerene edge

the potential drops suddenly to zero. This causes refraction which leads to an oscillating photoionization cross section. The refraction model assumed that the oscillation is of geometrical origin and a property of the entire valence electron density rather than due to individual quantum orbitals. Experimental data on other fullerenes [8] confirmed the original  $C_{60}$  experiments concerning the single frequency character of the oscillations. However, theoretical work [9] providing a general framework for geometry-based oscillations in photoionization cross sections for systems with delocalized electrons described by a jellium potential [10] predicted four oscillation frequencies when applied to  $C_{60}$ , connected to the diameter  $2R$  of  $C_{60}$ , to the thickness  $\Delta$  of the electron hull, and to sidebands related to  $2R \pm \Delta$  [11]. Previous experiments did not reach far enough in photon energy to clarify if these frequencies do exist.

Here, we report on new experimental data taken in smaller steps and at higher photon energies, as well as on new calculations designed to interpret as many features of the fullerene photoabsorption cross section as possible in structural terms. The measurements for the partial cross sections were performed at the undulator beam line BW3 of the Hamburg Synchrotron Radiation Laboratory HASYLAB at DESY [12]. This undulator delivers intense photon beams of  $\approx 10^{12}$  photons per sec, monochromatized by a SX 700 monochromator. The photon beam is crossed with an effusive beam of  $C_{60}$  molecules produced by a resistively heated crucible inside a vacuum chamber containing two time-of-flight (TOF) electron spectrometers for the energy and angular resolved detection of the  $C_{60}$  photoelectrons [6,8]. In order to keep the resolution of the electron spectra virtually the same for the whole energy range between 20 and 290 eV appropriate retardation voltages had to be applied before the electrons entered the drift tubes of the TOF spectrometers. The inset of Fig. 1 shows two of such spectra taken at a photon energy of 22 eV and 37 eV, respectively. A crucial point for the measurements is the calibration of the photon flux over the whole energy range

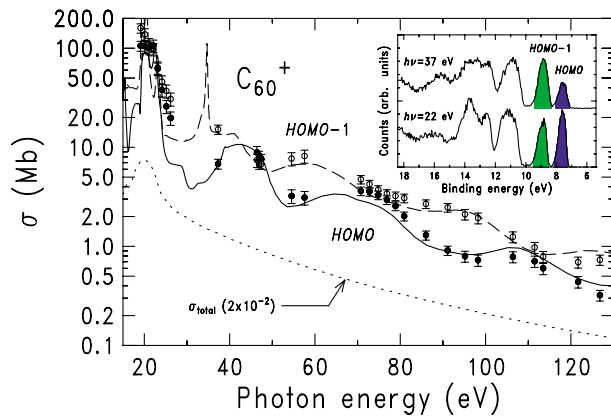


FIG. 1 (color online). Partial photoionization cross sections of the HOMO (filled circles) and HOMO - 1 (open circles) orbitals of  $C_{60}$ , between 18 and 130 eV photon energy. The dashed and solid curves represent the LDA calculations of Decleva *et al.* [13] using a full molecular potential. The dotted line represents the total photoionization cross section used for the normalization of the partial cross section. The inset displays two photoelectron spectra of  $C_{60}$ , taken at different photon energies showing the distinct intensity variation of the photolines of the two outermost orbitals HOMO and HOMO - 1.

in order to derive relative partial cross sections. They can be brought to an absolute scale by normalization to absorption measurements or by adoption of sum rules [14]. Such photon flux calibrated measurements were performed over an extended range of photon energies. The result is shown in the main part of Fig. 1 along with the total cross section and theoretical curves from a very recent *ab initio* calculation [13]. This calculation is based on an effective single particle description in the local density approximation (LDA), but it includes in addition to the spherical components of the potential anisotropic components of the full molecular potential [15]. The calculation agrees remarkably well with the experiment over the new extended energy regime, particularly with the new independent branching ratio measurements presented in Fig. 2.

To explore the prediction of four frequencies from the spherical-jellium model [11] we have set up a new calculation which contains an electronic level-dependent self-interaction correction [18]. In contrast to previous jellium-type descriptions, this produces the correct assignment of the angular momenta to the highest occupied levels as known from quantum chemical calculations. The photoionization amplitudes have been calculated in the framework of time-dependent local density approximation which also accounts for correlation in the final state through interchannel coupling; details will be published elsewhere. The total absorption cross section is in good agreement with experiment on an absolute scale if shifted in energy by 2.5 eV. This shift has also been reported comparing recent quantum chemical results to those of a

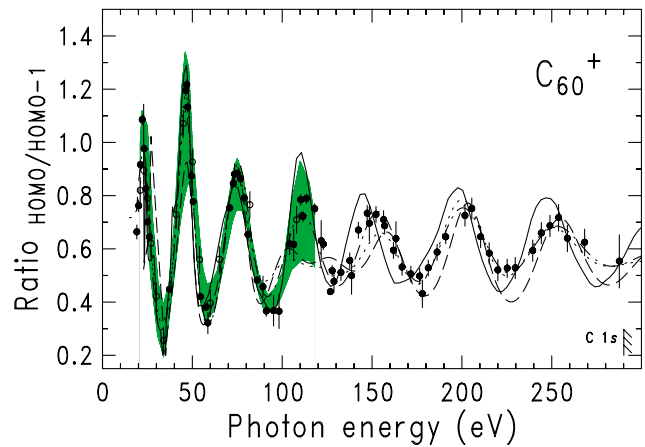


FIG. 2 (color online). Ratio of partial photoionization cross sections for the HOMO and HOMO - 1 (present data: filled black circles, former measurements [6]: open circles). The shaded area represents the various solid state measurements [5,16,17], whereas the different curves are the result of the discussed calculations (Decleva *et al.*: solid line; spherical-jellium model: dashed line; semiempirical: dash-dotted line; coherent part of the semiempirical fit: dotted line).

jellium based approach [19]. The cross section ratio from this calculation, shown in Fig. 2 as a dashed line, agrees with the overall oscillations and reproduces the (nontrivial) average ratio of about 0.55. However, there is clear disagreement with the experiment around 110 eV. This could be a consequence of artificial coherence induced by the spherical approximation of the jellium potential and not present in the nonspherical LDA calculation [13]. While in the nonspherical calculation the main frequency related to the diameter  $2R$  of the fullerene can be produced by many different radial potential components with different “width”  $\Delta_l \ll R$  belonging to different partial waves  $l$ , similarly as for the spherical-jellium model, no beating connected to  $\Delta$  will be generated as in the case of the spherical-jellium causing the depression of the signal around 110 eV. The latter effect can be modeled with a semiempirical fit based on rectangular potentials with a coherent part containing the shell width  $\Delta$  as parameter, an incoherent part giving rise to the  $R$ -dependent basic oscillation frequency and a smooth nonoscillatory background function  $B(h\nu)$  [20]. This fitting model accounts for both spherical-jellium and nonspherical molecularlike components of the effective potential, and it is able to quantify the contributions separately. This makes it possible to distinguish for the first time between localized and delocalized parts of the electron distribution in clusterlike systems. Figure 3 visualizes the complex interplay between the jellium picture with its spherically distributed delocalized electrons and the molecular orbital picture arising from the many nonspherical components of the molecular potential located near the carbon atoms of the  $C_{60}$  cage. The result of the fit to the experimental data with  $R = 0.354$  nm and

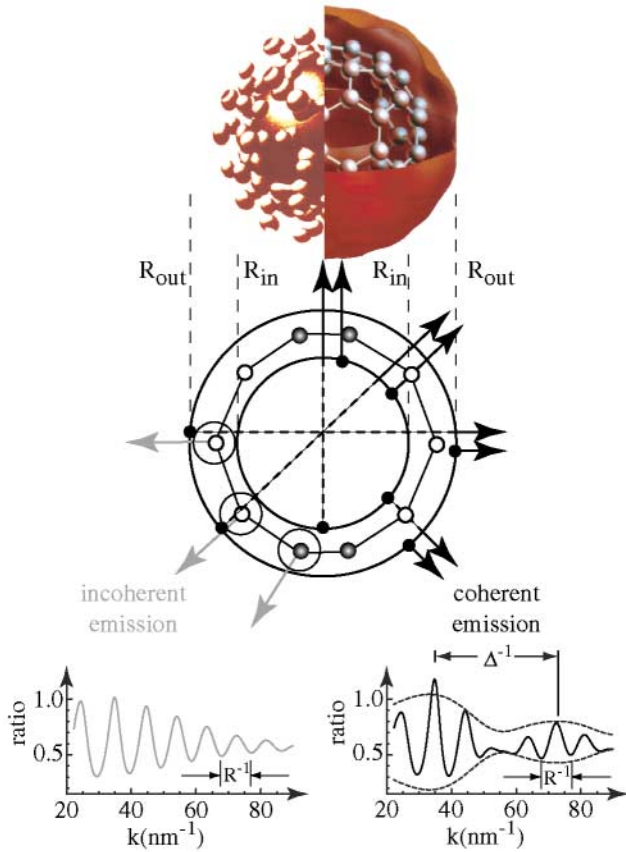


FIG. 3 (color online). Schematic representation of the  $\pi$ -electron distribution of the two outermost valence orbitals of  $C_{60}$  (Weaver and Poirier [3] and Bischof in Kuzmany's paper [21]) along with a cut through a spherical shell potential visualizing the way how coherent and incoherent photoemission from different parts of the fullerene, marked by filled and open circles, may occur. Two characteristic branching ratio oscillation patterns for each process over momentum vector  $\mathbf{k}$  are shown at the bottom of the figure. The geometric quantities  $R$  and  $\Delta$  are connected to the characteristic wavelengths  $\lambda_R$  and  $\lambda_\Delta$  via  $\pi/\lambda_{R,\Delta}$ .

$\Delta = 0.15$  nm is shown in Fig. 2 (dash-dotted curve). The coherent part of the cross section is plotted as a dotted line and, indeed, resembles the result of our spherical-jellium calculation closely. Although this is the first indication for additional frequencies originating from the edges of the potential, clear evidence is still masked by other noncoherent contributions. The new data set, however, taken in smaller steps over an extended range of photon energies ( $E_{\text{ph}} \gg E_{\text{bin}}$ ), allows us for the first time to perform a Fourier analysis with sufficient resolution to separate the various possible oscillation frequencies. The Fourier transform shown in Fig. 4 reveals indeed more than the one oscillation frequency corresponding to the diameter of  $C_{60}$ . One recognizes the right-hand side band belonging to the wavelength  $2R + \Delta$  and under the shoulder of the main peak the left side band at  $2R - \Delta$ ; only the low frequency beating, which represents the

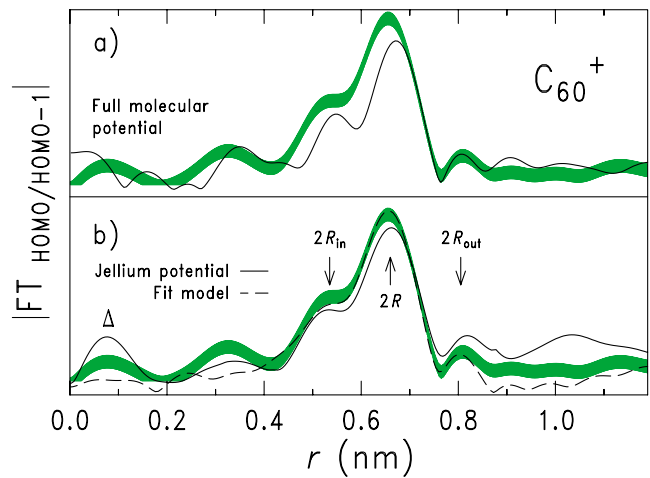


FIG. 4 (color online). Fourier transform of the cross section ratio in Fig. 3 for the experimental data (shaded area), the LDA calculation of Deleva *et al.* [solid line in (a)], the LDA calculation using a spherical-jellium potential [solid line in (b)], and the result of the semiempirical fit (dotted line) [22].

thickness  $\Delta$  of the electronic hull of  $C_{60}$ , is not pronounced in the Fourier spectrum. However, it can be quantitatively extracted from the difference between the main peak and the two sidebands. Note that besides the overestimation of the low frequency beating peak  $\Delta$  by the spherical-jellium model both calculations from Fig. 2 are in good agreement with the experiment concerning the main peaks of higher frequency. A non-negligible difference between the ideal theoretical jellium model and the real data is the finite temperature in the experiment. One might think that it does not influence data at high energies of 100 eV photon impact and more. However, the yield around the maximum of the cross section close to the plasmon at 20 eV contributes after convolution a tail even at higher energies, which constitutes a considerable background since the high energy cross section is exponentially small. In this context, another advantage of Fourier imaging becomes apparent: By Fourier transform the convolution integral is turned into a product of the Fourier transforms of the original signal and of the convolution function. Hence, the energy convolution has a substantial effect on the amplitudes of the oscillations, i.e., on the relative strengths of the peaks in the Fourier spectrum. However, the energy convolution does not influence the position of the peaks and therefore any results concerning the geometrical properties. This analysis shows that interference effects similar to those which have been observed recently in collisions with homonuclear molecules [23] do appear as well in the partial photoionization cross section, but not to the extent which one might expect on the basis of a pure spherical-jellium-type potential. As a consequence of this simplified potential, which consists of one spherical component only, the low frequency beating peak is overestimated.

Employment of a more realistic multicomponent potential [13] destroys the beating peak  $\Delta$ , while the higher frequency sidebands of the main peak are only broadened, but still clearly present. From the sidebands, the thickness  $\Delta$  of the electronic hull can be read off. More generally speaking, the complex aspects of the  $C_{60}$  electronic structure shown schematically in Fig. 3 give rise to the observed Fourier spectrum whose main features can be interpreted in terms of geometrical properties of the delocalized, but specifically structured, valence electron distribution.

In conclusion, we have demonstrated that photoionization cross section in Fourier reciprocal space is a proper tool to map out geometrical properties of valence electron distributions in many electron systems. This is due to the sensitivity of the dipole operator on the gradient of the effective potential. In principle, this type of imaging should be possible for all systems with a large number of delocalized electrons. First results on the less spherical system  $C_{70}$  corroborate this expectation. However, the present pilot investigation has been possible only thanks to the unique properties of  $C_{60}$ . Its spherical symmetry allowed us to use all molecules from the beam without having to orient them, and effusive  $C_{60}$  beams produced by evaporation reached a relatively large density compared, e.g., to other cluster beams. The high intensity of the target beam was necessary since the cross sections become exponentially small towards large photon energies. These types of experiments and hence this imaging will become feasible for other target systems, such as mass selected clusters, by using more intense radiation available from x-ray free electron lasers in the near future.

We thank Piero Decleva for helpful discussions and for providing us with his theoretical data prior to publication. We are also thankful to Burkhard Langer and Evelyn Prohn for their help in preparing the figures.

\*Electronic address: becker\_u@fhi-berlin.mpg.de

†Present address: Department of Physics, 116 Cardwell, Kansas State University, Manhattan, KS 66506.

- [1] H. Kroto, J. Heath, S. O'Brien, R. Curl, and R. Smalley, *Nature* (London) **318**, 162 (1985).
- [2] D. J. Hornbaker, S.-J. Kahng, S. Misra, B. W. Smith, A. T. Johnson, E. J. Mele, D. E. Luzzi, and A. Yazdani, *Science* **295**, 828 (2002).
- [3] J. Weaver and D. Poirier, in *Solid State Physics*, edited by H. Ehrenreich and F. Spaepen (Academic Press, Cambridge, 1994), p. 1.
- [4] S. Krummacher, M. Biermann, M. Neeb, A. Liebsch, and W. Eberhardt, *Phys. Rev. B* **48**, 8424 (1993).
- [5] P. Benning, D. Poirier, N. Troullier, J. Martins, J. Weaver, R. Haufler, L. Chibante, and R. Smalley, *Phys. Rev. B* **44**, 1962 (1991).
- [6] T. Liebsch, O. Plotzke, F. Heiser, U. Hergenhanh, O. Hemmers, R. Wehlitz, J. Viefhaus, B. Langer, S. B. Whitfield, and U. Becker, *Phys. Rev. A* **52**, 457 (1995).
- [7] Y. B. Xu, M. Q. Tan, and U. Becker, *Phys. Rev. Lett.* **76**, 3538 (1996), and references therein.
- [8] T. Liebsch, R. Hentges, A. Rüdell, J. Viefhaus, U. Becker, and R. Schlögl, *Chem. Phys. Lett.* **279**, 197 (1997).
- [9] O. Frank and J. M. Rost, *Phys. Rev. A* **60**, 392 (1999).
- [10] W. Ekardt, *Phys. Rev. Lett.* **52**, 1925 (1984).
- [11] O. Frank and J. Rost, *Chem. Phys. Lett.* **271**, 367 (1997).
- [12] C. U. S. Larsson, A. Beutler, O. Björneholm, F. Federmann, U. Hahn, A. Rieck, S. Verbin, and T. Möller, *Nucl. Instrum. Methods Phys. Res., Sect. A* **337**, 603 (1994).
- [13] P. Decleva, S. Furlan, G. Fronzoni, and M. Stener, *Chem. Phys. Lett.* **348**, 363 (2001), and references therein.
- [14] J. Berkowitz, *J. Chem. Phys.* **111**, 1446 (1999).
- [15] M. Venuti, M. Stener, G. D. Alti, and P. Decleva, *J. Chem. Phys.* **111**, 4589 (1999).
- [16] J. Wu, Z. Shen, D. Dessau, R. Cao, D. Marshall, P. Pianetta, I. Lindau, X. Yang, J. Terry, D. King, B. Wells, D. Elloway, H. Wendt, C. Brown, H. Hunziker, and M. de Vries, *Physica* (Amsterdam) **197C**, 251 (1992).
- [17] S. Hasegawa, T. Miyamae, K. Yashuki, H. Inokuchi, K. Seki, and N. Ueno, *Phys. Rev. B* **58**, 4927 (1998).
- [18] M. E. Madjet, H. S. Chakraborty, and J. M. Rost, *J. Phys. B* **34**, L345 (2001).
- [19] F. A. Gianturco and R. R. Lucchese, *Phys. Rev. A* **64**, 032706 (2001).
- [20] The partial cross sections are calculated as  $\sigma_l(h\nu) \propto F_l(h\nu)(|j_{l\pm 1}^{R-\delta}(h\nu) + j_{l\pm 1}^{R+\delta}(h\nu)|^2 + C|j_{l\pm 1}^R(h\nu)|^2) + B(h\nu)$ , where  $l = 5$  for HOMO and  $l = 4$  for HOMO - 1, respectively,  $F$  being a photon energy dependent damping function,  $j_l$  being a spherical Bessel function of order  $l$ , and  $C$  being a constant defining the incoherent portion of the cross sections.
- [21] H. Kuzmany, *Phys. Z.* **29**, 16 (1998).
- [22] The geometric properties of the  $C_{60}$  potential are not directly displayed by the peak positions in the plotted Fourier spectrum; they correspond rather to the asymptotic frequencies  $\ell_{\gg 1}^{-1}$  being proportional to the energy window dependent spectral frequency  $\ell^{-1}$ . The photoelectron cutoff energy of 280 eV used in the present study corresponds to a proportionality factor of 1.085.
- [23] N. Stolterfoht, B. Sulik, V. Hoffmann, B. Skogvall, J. Y. Chesnel, J. Rangama, F. Frémont, D. Hennecart, A. Cassimi, X. Husson, A. L. Landers, J. A. Tanis, M. E. Galassi, and R. D. Rivarola, *Phys. Rev. Lett.* **87**, 023201 (2001).